Biology Direct

RESEARCH

Open Access

E3 ligase HERC5-catalyzed UGDH isgylation promotes SNAI1-mediated tumor metastasis and cisplatin resistance in oral squamous cell carcinoma

Xu Zhang[1], Fayu Liu[2], Qigen Fang[1], Changfu Sun[2] and Jie Fan[1*]

Abstract

Background Oral squamous cell carcinoma (OSCC) is one of the leading causes of cancer-related mortality worldwide due to its high aggressive potential and drug resistance. Previous studies have revealed an important function of HECT And RLD Domain Containing E3 Ubiquitin Protein Ligase 5 (HERC5) in cancer. Six GEO gene microarrays identified HERC5 as a significant upregulated gene in OSCC tissues or cells (log2 Fold change > 1 and adj.$p < 0.05$). This study aimed to explore the role and underlying mechanisms of HERC5 in OSCC development.

Results High HERC5 expression in OSCC tissues was confirmed by our hospital validation cohort and positively correlated with primary tumor stages. Subsequent functional studies demonstrated that knockdown of HERC5 inhibited the migratory and invasive capabilities with decrease of Vimentin and increase of E-cadherin in OSCC cells. In cisplatin treatment, cell survival rates were significantly reduced in HERC5-silencing OSCC cells, accompanied by the increase in cytotoxicity, DNA damage and apoptosis. OSCC cell-derived tumor xenograft displayed that HERC5 depletion inhibited pulmonary metastasis as well as restored the cisplatin-induced tumor burden. In line with this, overexpression of HERC5 yielded the opposite alterations both in vivo and in vitro. Mechanistically, UDP-glucose 6-dehydrogenase (UGDH) was identified as a HERC5-binding protein. Cysteine residue at position 994 in the HECT domain of HERC5 catalyzed the conjugation of ubiquitin-like protein Interferon-induced 15 kDa protein (ISG15) to UGDH (ISGylation of UGDH) and facilitated its phosphorylation, therefore enhancing SNAI1 mRNA stability. SNAI1 depletion inhibited HERC5 overexpression-triggered invasion and cisplatin resistance of OSCC cells.

Conclusions Our study indicates that HERC5 may be a promising therapeutic target for OSCC.

Keywords HERC5, Oral squamous cell carcinoma, Metastasis, Cisplatin sensitivity, ISGylation, UGDH

*Correspondence:
Jie Fan
zlyyfanjie4235@zzu.edu.cn
[1]Department of Head Neck and Thyroid, The Affiliated Cancer Hospital of Zhengzhou University & Henan Cancer Hospital, No. 127, Dongming Road, Zhengzhou, China
[2]Department of Oromaxillofacial-Head and Neck Surgery, School and Hospital of Stomatology, Liaoning Province Key Laboratory of Oral Disease, China Medical University, Shenyang, China

Background

Oral squamous cell carcinoma (OSCC) is one of the frequently common malignancy and accounts for more than 95% of head and neck cancers (HNC) [1]. Tobacco smoking, alcohol, betel quid chewing, and human papillomavirus infection linked to certain sexual behaviors are the major risk factors for OSCC. It arises anywhere in the oral cavity, as well as usually causes difficulty in chewing and swallowing, recurrent ulcers, and worsens patients' quality of life. OSCC has aggressive potential due to innate and acquired chemoresistance, thereby resulting in adverse prognosis. The overall 5-year survival rate of OSCC has not reached 50% for the last decades [2]. Elucidating the molecular mechanism of OSCC is imperative for early detection and treatment, improving patient survival.

Interferon-induced 15 kDa protein (ISG15), a ubiquitin-like protein, is expressed in a wide variety of cell types. ISG15 exists both intracellularly and extracellularly in free form, or covalently conjugate to other proteins via ISGylation to regulate immunity and tumor development. Like ubiquitylation, ISGylation is a 3-step enzymatic cascade that requires the E1 enzyme Ubiquitin Like Modifier Activating Enzyme 7 (UBA7; also UBE1L), the E2 enzyme Ubiquitin Conjugating Enzyme E2 L6 (UBE2L6; also UBCH8), and the E3 ligases, which in humans is mainly HECT And RLD Domain Containing E3 Ubiquitin Protein Ligase 5 (HERC5) [3]. ISGylation exerted both tumor-promoting and tumor-suppressive effects by regulating protein stability or activity through crosstalk with other post-translational modifications. For example, ISGylation triggered breast tumor progression by increasing Akt phosphorylation level [4]. ISGylation inhibited YAP proteasome degradation via antagonizing the ubiquitin pathway in lung cancer cell lines [5]. In contrast, Mustachio et al. found that ISGylation of tumor suppressor PTEN reduced its stability and therefore limited tumor-inhibitory ability [6]. In addition to its role in protein covalently binding, ISG15 could promote or inhibit progression of different cancers in the form of monomers [7, 8]. Chen et al. found that ISG15 facilitated migration of OSCC cells in an ISGylation-independent manner [9]. Whether the covalent binding of ISG15 to target proteins was involved in the occurrence and development of OSCC remains unknown.

Well-known HERC5-catalyzed ISGylation promoted nucleotidyl-transferase oligomerization and enhanced its enzymatic activity, thereby boosting the antiviral innate immunity [10]. In addition to its well-established role in antiviral immunity, HERC5 has been reported to regulate cancer development. Highly expressed HERC5 accelerated cell proliferation and/or migration of breast cancer and hepatocellular carcinoma [11, 12]. HERC5 was also considered to be a gene that drove cisplatin resistance in ovarian cancer cells [13]. In human papillomavirus (HPV)-positive oropharyngeal cancer, overexpression of HERC5 in OSCC patients exhibited a worse prognosis [14]. Analyzing transcriptome profiles of cancerous and normal tissues, we noted that HERC5 was upregulated in OSCC tissues. Therefore, we speculated that HERC5 might be involved in OSCC tumorigenesis by its ISGylation function.

UDP-glucose 6-dehydrogenase (UGDH) is a key enzyme in the uronic acid pathway, and converts UDP-glucose (UDP-Glc), an active form of glucose, to UDP-glucuronic acid (UDP-GlcUA) [15]. UDP-GlcUA is an indispensable precursor for the synthesis of glycosaminoglycans that provides structural support for cells, as well as promotes cell migration and wound healing. UGDH has been reported to be implicated in tumor growth and migration. Knockout of UGDH inhibited migration and reduced in vivo metastatic ability of breast cancer cells [16]. Silencing of UGDH also delayed glioblastoma cell proliferation and migration in vitro [17]. A paper published in *Nature* journal revealed that phosphorylation of UGDH at tyrosine 473 (pUGDH(Y473)) contributed to lung cancer metastasis via enhancing stability of EMT-inducer SNAI1 mRNA [18]. Increased SNAI1 was previously reported to reduce cisplatin sensitivity in head and neck squamous cell carcinoma [19]. Cancer Proteogenomic Data Analysis Site (cProSite) database displayed enhanced pUGDH(Y473) level, while total protein abundance was not changed in HNC. These findings indicated that activation of UGDH might exert a tumor-promoting role in OSCC.

In the present study, we sought to uncover the role of HERC5 in OSCC development. Gain-of-function and loss-of-function experiments were performed to investigate its role in the migration, invasion, and cisplatin sensitivity of OSCC cells and cell-derived tumor xenografts. Furthermore, whether HERC5-catalyzed ISGylation affected UGDH activity and subsequent SNAI1 mRNA stability in OSCC were tested.

Methods

Acquisition of gene expression datasets

Gene expression datasets used in this study were downloaded from Gene Expression Omnibus (GEO) database (accession number: GSE30784, GSE160042, GSE3524, GSE74530, GSE9844, GSE21866, and GSE31056).

Screening for differentially expressed genes (DEGs)

To identify DEGs in OSCC, an online tool GEO2R provided by the GEO database officially was used to compare two or more groups of samples in a GEO Series.|log2 [Fold change (FC)]| > 1 and adj.$p < 0.05$ were regarded as cut off. A Venn diagram was drawn by package venn (version 1.12) to obtain common DEGs.

Identification of hub genes

To analyze protein interaction information, the common DEGs were uploaded to STRING online database to obtain a protein-protein interaction (PPI) network. According to the number of gene connections or degrees, hub genes from the PPI network were identified using Cytoscape software (version 3.9.1).

Patients and tissue samples

Fresh frozen and paraffin-embedded tumor and the matched paracancerous tissues from OSCC patients were provided by the Henan Cancer Hospital. None of these patients had received radiotherapy or chemotherapy before their surgery. Primary tumor (T) stages were determined on the base of the AJCC 8th Edition Cancer Staging Manual. Sample processing was performed following standard operating procedures with the approval by the Ethical and Scientific Committees of Henan Cancer Hospital (No. 2022-07-01), and obtained informed consent. Expression of HERC5 mRNA and protein in the frozen tissue samples from 32 OSCC patients was determined by real-time PCR and western blot analyses. The paraffin-embedded samples from OSCC patients were used for immunohistochemistry staining of HERC5.

Immunohistochemistry

The paraffin-embedded tissues were cut into 5 μm sections, placed on slides, and heated to 60 °C for 2 h. The sections were dewaxed with xylenes and rehydrated through graded concentrations of ethanol. The sections were subjected to antigen retrieval using citrate buffer in conjunction with heat supplied by a microwave oven for 10 min and then cooled to room temperature. The sections were incubated with 3% hydrogen peroxide and blocked with 1% bovine serum albumin (BSA). Subsequently, the tissue sections were incubated with an anti-HERC5 antibody (22692-1-AP; ProteinTech, Rosemont, Illinois, USA [1:200 dilution]) overnight at 4 °C. After washing, the sections were treated with a horseradish peroxidase (HRP)-conjugated goat anti-rabbit IgG secondary antibody (#31460, Thermo Fisher Scientific, Karlsruhe, Germany [1:500 dilution]) at 37 °C for 60 min. Finally, the sections were stained with diaminobenzidine, counterstained with hematoxylin, dehydrated in ethanol, cleaned in xylene and mounted. Images were captured using an Olympus BX53 microscope fixed with a DP73 digital color camera under 200× magnification.

Cancer cell line encyclopedia (CCLE)

CCLE database provides data on gene expression in 1000 human cancer cell lines. Target gene expression in five OSCC cell lines (CAL27, SCC25, SAS, SCC4, and SCC9) was analyzed using the CCLE database.

Cell culture

Human OSCC cell lines CAL27 and SCC9 cells were kindly provided by iCell Bioscience (Shanghai, China). CAL27 cells were maintained in DMEM (G4511, Servicebio, Wuhan, China) supplemented with 10% BSA in a humidified atmosphere with 5% CO_2 at 37 °C. SCC9 cells were cultured in DMEM/F12 (BL305A, Biosharp, Hefei, China) containing 10% BSA at 37 °C, 5% CO_2.

Plasmid construction and transfection

pCDNA3.1-CMV/eGFP and pGCsi-H1/Neo/GFP plasmids were used for overexpression and silencing of HERC5. For HERC5 overexpression, HERC5 CDS (NM_016323) was inserted into the pCDNA3.1-CMV/eGFP plasmid to construct pCDNA3.1-CMV/eGFP-HERC5, named HERC5 and empty plasmid (EP). SCC9 cells were transfected with HERC5 and EP using Lipofectamine 3000 (L3000015, Invitrogen, Thermo Fisher Scientific) following the manufacturer's protocol. Forty-eight h later, 150 mg/ml G418 (Invitrogen) was added into SCC9 cultures for the selection of stably transfected cells. The cells were cultured in G418-containing medium for two weeks with the medium refreshed every other day. Subsequently, two stable clones with better transfection efficiency were picked and expanded, named HERC5_cl#A and HERC5_cl#B, respectively. For HERC5 silencing, according to the efficiency of knockdown for four siRNA sequences targeting HERC5 mRNA, two HERC5-specific shRNAs (target sequence#1, 5'-GGAGAAUGGUAAUGUUCAA-3'; sequence#2, 5'-CGACGAAGACAUUAUCAAA-3') and non-targeting control (NC) shRNA were designed for follow-up generation of stable knockdown cell lines. The shRNAs were inserted into the pGCsi-H1/Neo/GFP plasmids to construct pGCsi-H1/Neo/GFP-HERC5 shRNA#1, pGCsi-H1/Neo/GFP-HERC5 shRNA#2 and pGCsi-H1/Neo/GFP-NC shRNA, named HERC5_shR#1, HERC5_shR#2, and NC_shR, respectively. The plasmids were then transfected into the CAL27 cells using Lipofectamine 3000. Forty-eight h later, 150 mg/ml G418 (Invitrogen) was added into CAL27 cultures for the selection of stably transfected

cells. The cells were cultured in G418-containing medium for two weeks with the medium refreshed every other day. Subsequently, the best stable clones were picked and expanded. Expression of HERC5 in the stable strains was determined by real-time PCR analysis. Schematic diagram for plasmid construction and transfection were shown in Fig. 1B-C.

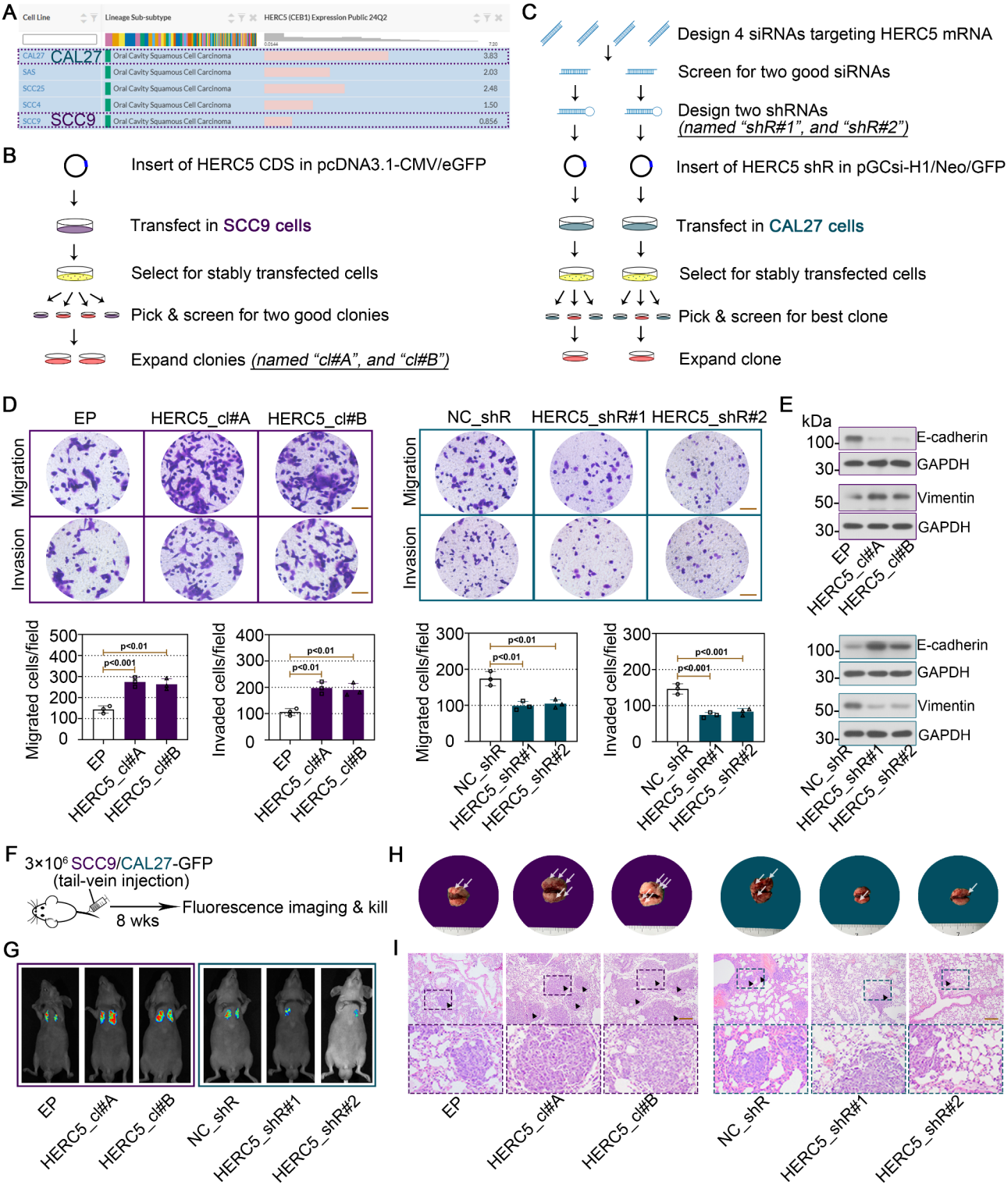

Fig. 1 (See legend on next page.)

(See figure on previous page.)

Fig. 1 Anti-metastatic role of HERC5 silencing in OSCC cells in vitro and in vivo. (**A**). Expression levels of HERC5 mRNA in five OSCC cells (CAL27, SCC25, SAS, SCC4, and SCC9 in descending order of expression levels) from the Cancer Cell Line Encyclopedia (CCLE) dataset. (**B**). HERC5 CDS fragments were inserted in pcDNA3.1-CMV/eGFP plasmid. SCC9 cells were transfected with pcDNA3.1-CMV/eGFP-HERC5 or pcDNA3.1-CMV/eGFP (empty plasmid, EP), followed by selection of stably transfected cells and isolation of stable clones, named HERC5_cl#A, HERC5_cl#B and EP. (**C**). Two shRNAs targeting HERC5 mRNA and non-targeting control (NC) shRNA were inserted in pGCsi-H1/Neo/GFP plasmid. CAL27 cells were transfected with pGCsi-H1/Neo/GFP-HERC5 shRNA or pGCsi-H1/Neo/GFP-NC shRNA, followed by selection of stably transfected cells and isolation of stable clones, named HERC5_shR#1, HERC5_shR#2 and NC_shR. (**D**). Transwell migration and matrigel invasion assays in SCC9 (left) or CAL27 (right) cells. Representative photomicrographs and quantification of the migratory or invasive cells (stained with crystal violet) at 24 h in lower surface of Transwell chamber. Scale bars: 100 μm. (**E**). Representative results of western blot analyses for E-cadherin and Vimentin in SCC9 (up) or CAL27 (down) cells. (**F**). Schematic diagram for tail-vein injection of 3×10^6 stably transfected SCC9 or CAL27 cells marked with GFP into Balb/C nude mice for 8 weeks. (**G**). In vivo GFP fluorescence imaging of the mice with lung metastasis 8 weeks after tail-vein injection of SCC9 (left) or CAL27 (right) cells. (**H**). Representative photos of lungs from the mice 8 weeks after tail-vein injection of SCC9 (left) or CAL27 (right) cells. Arrow denotes visible metastatic nodules presented in the lungs. (**I**). Representative H&E images of lung tissues from the mice after tail-vein injection of SCC9 (left) or CAL27 (right) cells. Arrowhead denotes lung metastatic foci. Scale bars: 200 μm. Data in (D) were expressed as mean values ± SD

For knocking down UGDH or SNAI1, a shRNA targeting 5'-GGUUGUUGAUGUCAAUGAA-3' of UGDH mRNA or targeting 5'-GAAUGUCCCUGCUCCACAA-3' of SNAI1 mRNA was inserted into pRNA-H1.1/Neo plasmid. Afterward, the plasmids were transiently transfected into stably expressed SCC9 cells.

To determine the effect of HERC5 on UGDH ISGylation, SCC9 cells were transiently transfected with pcDNA3.1 plasmids of C-terminally Myc-tagged HERC5 (wild type or Cys994Ala point mutation), C-terminally Flag-tagged UGDH and C-terminally HA-tagged ISG15, using Lipofectamine 3000 following the manufacturer's protocol.

To determine the effect of HERC5-mediated ISGylation on UGDH tyrosine phosphorylation, SCC9 cells were transiently transfected with pcDNA3.1 plasmids of C-terminally Myc-tagged HERC5, C-terminally Flag-tagged UGDH (wild type or Tyr473Phe point mutation) and C-terminally HA-tagged ISG15, using Lipofectamine 3000 following the manufacturer's protocol.

Cell proliferation assay

Cells were seeded on 96-well plates at a density of 1×10^4 cells/well. Subsequently, the cells were treated with various concentrations (0, 1.25, 2.5, 5, 10, 20, 40, 80 and 160 μM) of cisplatin (#MB1055, Meilun Biotech Co., Ltd (Dalian, China). A tetrazolium dye (MTT, KGA9301, KeyGene Biotech., Nanjing, China) detection kit was applied to examine the cytotoxicity of cisplatin after 48 h of treatment, according to the supplier's instructions. The optical density (OD) of each well was detected at a wavelength of 490 nm. The percentage of cell mortality was then calculated by the formula $(1\text{-}OD_{X\ \mu M}/OD_{0\ \mu M})\times100\%$.

Detection for lactate dehydrogenase (LDH) release

Cytotoxicity of cisplatin was evaluated based on th LDH release. LDH content was detected both in the medium and cell lysate using an ELISA kit (SEB864Hu, Cloud-Clone Corp., Katy, TX, USA) following the manufacturer's protocol. LDH release was calculated as the ratio of LDH content in the medium and the total LDH content (medium + lysate).

In vivo study

All animal experiments were conducted according to the Principles of Laboratory Animal Care and approved by the Institutional Animal Care and Use Committee of Henan Cancer Hospital. Male Balb/C nude mice aged 6 weeks were purchased from Huachuang Sino (Jiangsu, China) and housed in a standard environment on a 12-h light/dark cycle, 22 ± 1 °C temperature and 45–55% humidity. All animals had free access to food and water. For the pulmonary metastasis assay, 3×10^6/0.1 ml stably expressed SCC9 and CAL27 cells marked with green fluorescent protein (GFP) were injected into the tail vein of nude mice. After 8 weeks, lung metastases in mice were visualized by fluorescence imaging. Subsequently, mice were sacrificed. Lungs were collected, paraffin-embedded, sectioned, and stained with hematoxylin and eosin (H&E). The staining images of lung tissues were captured using the Olympus BX53/DP73 microscope under 100× magnification.

To evaluate the tumorigenicity of HERC5 upon cisplatin treatment, SCC9 and CAL27 cells were applied for tumor xenografts. Mice were inoculated subcutaneously into 2×10^6/0.1 ml OSCC cells. When the xenograft grew to ~50 mm^3, mice were intraperitoneally injected 3 mg/kg of cisplatin twice weekly. Tumor volume was measured every three days using the following formula: $length\times width^2\times0.5$. After 3 weeks, mice were sacrificed, and tumors were excised, weighed.

Real-time polymerase chain reaction (Real-time PCR)

Total RNA from the tissue samples or cells was isolated by TRIpure reagent (RP1001, BioTeke Bio., Beijing, China). One microgram of RNA was used for cDNA synthesis using All-in-One First-Strand SuperMix according to manufacturer's instructions (MD80101, Magen Bio., Guangzhou, China). Real-time PCR was performed on ExicyclerTM 96 Real-Time Quantitative Thermal Block (Bioneer, Daejeon, South Korea) using cDNA, 2×Taq

PCR MasterMix (PC1150, Solarbio Life Sciences, Beijing, China), SYBR green (SR4110, Solarbio) and primers. The primer sequences were shown below: homo HERC5 forward, 5'-GAAGCTGCACAGGGTAAA-3' and reverse, 5'-GAAGCGTCCACAGTCATT-3'; homo SNAI1 forward, 5'-GTTTACCTTCCAGCAGCCCTAC-3' and reverse 5'-GCCTTTCCCACTGTCCTCAT-3'. The reaction consisted of an initial 5 min denaturation step at 95 °C followed by 40 cycles of denaturation (10s at 95 °C), annealing (10s at 60 °C) and extension (15s at 72 °C). Relative gene expression in cells was calculated using $2^{-\Delta\Delta CT}$ method and gene expression in tissues for $2^{-\Delta CT}$ method. GAPDH served as an internal reaction control to normalize mRNA levels.

For mRNA stability assay, cells were pretreated with actinomycin D at the indicated times, followed by real-time PCR analysis. Data were normalized to expression of a control gene ribosomal protein S18 (RPS18).

Co-immunoprecipitation (Co-IP) assay

Whole-cell extracts (WCE) were obtained in IP lysis buffer (R0030, Solarbio). After centrifugation at 10,000 g at 4 °C for 5 min, protein concentrations were detected using a bicinchoninic acid (BCA) assay kit (PC0020, Solarbio). The supernatants were incubated with IP-specific antibodies at 4 °C overnight, after which cultured with Protein A plus G agarose beads (PR40025, ProteinTech) at 4 °C for 4 h. The details of IP-specific antibodies were as follows: anti- Pan Phospho-Tyrosine (AP1162, ABclonal), anti-HERC5 (22692-1-AP, ProteinTech), anti-ISG15 (15981-1-AP, ProteinTech), and anti-HA (51064-2-AP, ProteinTech). Subsequently, the immunoprecipitates were analyzed by western blot assay.

Western blot

Total proteins from the tissue samples or cells were extracted in RIPA buffer (R0010, Solarbio) supplemented with PMSF protease inhibitor (P0100, Solarbio). After five min of centrifugation at 10,000 g at 4 °C, protein concentrations in the lysates were measured with the BCA assay. Ten to twenty micrograms of lysates were resolved by sodium dodecyl sulfate-polyacrylamide gel electrophoresis (SDS-PAGE) and transferred to PVDF membranes. The membranes were treated with blocking buffer (SW3010, Solarbio), followed by incubation in a 1:1000 dilution of indicated primary antibodies: anti-HERC5 antibody (22692-1-AP, ProteinTech), anti-E-cadherin antibody (AF0131, Affinity, Cincinnati, OH, USA), anti-Vimentin antibody (AF7013, Affinity), anti-cleaved PARP antibody (AF7023, Affinity), anti-γ-H2AX Ser139 antibody (AF3187, Affinity), anti-SNAI1 antibody (AF6032, Affinity), anti-UGDH antibody (sc-137058, Santa Cruz Biotechnology, Santa Cruz, CA, USA), anti-Flag antibody (66008-4-Ig, ProteinTech), anti-Myc antibody (AE070, ABclonal [1:10000 dilution]), and anti-GAPDH antibody (60004-1-Ig, ProteinTech [1:10000 dilution]) overnight at 4 °C. After washing, the membranes were incubated with HRP-conjugated goat anti-rabbit IgG (SE134, Solarbio) or goat anti-mouse IgG (SE131, Solarbio) antibody. Protein bands were visualized using enhanced chemiluminescent substrate (PE0010, Solarbio).

Transwell migration and matrigel-invasion assays

Cells suspended in 200 µl of serum-free culture medium were added into the upper chamber of a Transwell filter with 8-µm pores (14341, Labselect, Hefei, China), while 800 µl of 10% FBS medium was added to the lower chamber in a 24-well plate. For invasion assay, Transwell filters were precoated with Matrigel (356234, Corning, Cambridge, MA, USA) to mimic in vitro biological matrix barriers. After incubation for 24 h, the cells that remained on the upper surface of the filter were wiped off. The cells that had crossed the filter and adhered on the lower surface were stained with 0.5% crystal violet for 5 min. Images of the stained lower surface were captured, and the cells were quantified under a microscope in five random fields at 200× magnification.

Flow cytometry

Cell apoptosis was analyzed by flow cytometry. Cells were collected after centrifugation at 150 g for 5 min, washed twice with PBS, as well as stained using PE-labelled Annexin V and 7-AAD according to the manufacturer's instructions (G152, Servicebio). Stained cells were analyzed using a NovoCyte Flow Cytometer (Agilent, Santa Clara, CA, USA). The percentage of apoptosis was calculated by the sum of early apoptotic cells (Annexin V-PE^+/7-AAD^-) and late apoptotic cells (Annexin V-PE^+/7-AAD^+).

Statistical analyses

GraphPad Prism version 8.0.2 for Windows 11 was used for all analyses. Data passed any of the standard normality tests, including Anderson-Darling test, D'Agostino & Pearson test, Shapiro-Wilk test and Kolmogorov-Smirnov test, were analyzed with two-tailed Student's t test (unpaired and paired), one-way or two-way ANOVA followed by Tukey's or Sidak's multiple comparison test. Data unpassed the normality test were analyzed with Mann Whitney test or Wilcoxon matched-pairs signed rank test. Statistical significance was set at $P < 0.05$. Data were presented as means ± standard deviations (SDs). IC_{50} is defined as the concentration of drug which results in exactly half of the maximum inhibition effect for cell proliferation. IC_{50} values were calculated using logarithmically transformed followed by nonlinear regression.

Results

HERC5, an ISG15-conjugating protein, is up-regulated in OSCC tissues

Using the publicly available transcriptome datasets (GSE30784, GSE160042, GSE3524, GSE74530, GSE9844, and GSE21866), we analyzed genes that were differentially expressed in OSCC tissues/cells versus normal tissues/oral keratinocytes with the screening criteria of|log2 FC| > 1 and adj.$p < 0.05$. The Venn diagram was shown in Figs. 2A and 14 DEGs (ISG15,

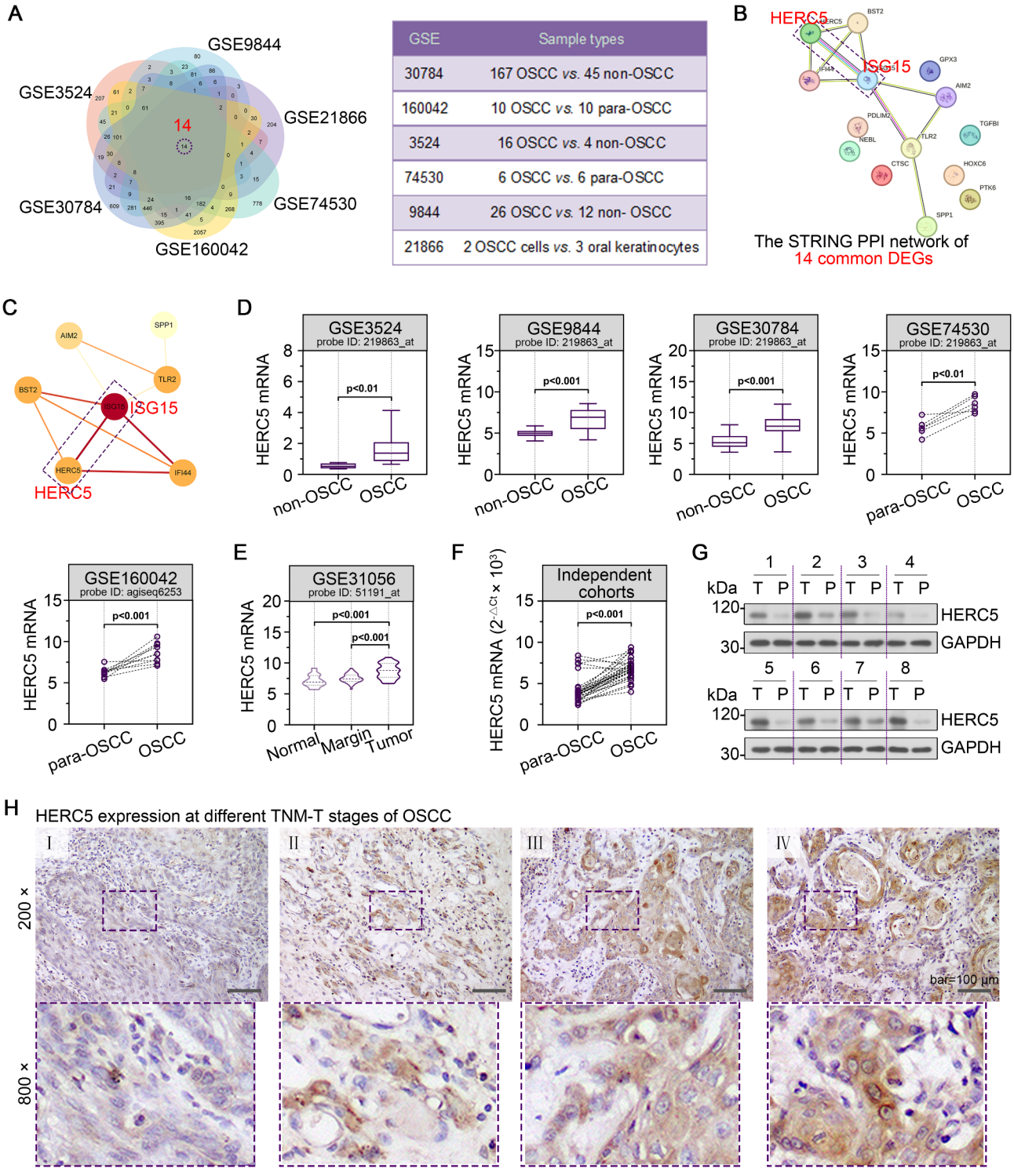

Fig. 2 (See legend on next page.)

(See figure on previous page.)

Fig. 2 HERC5, an ISG15-conjugating protein, is up-regulated in OSCC tissues. (**A**). Venn diagrams of differentially expressed genes (DEGs) with|log2 [Fold change (FC)]| > 1 and adj.$p < 0.05$ in GSE30784, GSE160042, GSE3524, GSE74530, GSE9844, and GSE21866 datasets. A total of 14 common DEGs were presented. (**B**). The interactive relationship of 14 common DEGs was analyzed and displayed as protein-protein interaction (PPI) network by STRING website. (**C**). The hub genes of PPI network were recognized by the Cytoscape software based on the connection degree and presented as circle. The colors of the circles were presented from red to yellow in descending order of degree values. The line thickness and color connecting two circles illustrated the strength of the interaction between nodes. (**D**). HERC5 mRNA expression levels in OSCC tissues and normal oral/paracancerous tissues of GSE30784, GSE160042, GSE3524, GSE74530, and GSE9844 datasets. (**E**). HERC5 mRNA expression levels in normal, margin, and tumor core of a GSE31056 dataset. (**F**). HERC5 mRNA expression levels in 32 paired OSCC and para-OSCC tissues of our independent hospital cohorts. (**G**). HERC5 protein expression levels in 8 paired OSCC and para-OSCC tissues from our independent hospital cohorts. P, para-OSCC tissues. T, OSCC tissues. (H). HERC5 expression in OSCC tissues at different TNM-T stages by immunohistochemistry. Brown grains represented positive signals. Scale bars: 100 μm. Data in (D) were expressed as mean values ± SD

HERC5, GPX3, CTSC, TGFBI, BST2, NEBL, TLR2, PTK6, AIM2, HOXC6, SPP1, IFI44, and PDLIM2) were found consistently significantly differentially expressed in six datasets. Of the 14 DEGs, 10 (ISG15, HERC5, CTSC, TGFBI, BST2, TLR2, AIM2, HOXC6, SPP1, and IFI44) were commonly overexpressed in OSCC, while 4 (GPX3, NEBL, PTK6, and PDLIM2) were lowly expressed. Aiming at visualizing the gene lists and interactions, 14 DEGs and their interactions between each other were displayed in a PPI network with STRING (Fig. 2B). A total of 7 hub genes (ISG15, HERC5, BST2, IFI44, TLR2, AIM2, and SPP1) in the PPI network were recognized by the Cytoscape software (Fig. 2C). ISG15 was the top 1 hub gene with the highest number of gene connections or degrees. As expected, HERC5 as a core E3 ligase of ISG15-conjugating system had the strongest interaction with ISG15 (Fig. 2C).

Next, HERC5 transcriptional levels in OSCC tissues were specified by the above datasets. As shown in Fig. 2D, expression of HERC5 mRNA was significantly up-regulated in tumor samples versus normal or paracancerous tissues. In addition, HERC5 mRNA levels were gradually elevated in normal oral tissues, margins and OSCC tissues of a GSE31056 dataset (Fig. 2E). We performed real-time PCR validation of HERC5 expression in OSCC and para-OSCC tissues from our hospital cohort of 32 patients. This validation analysis confirmed that HERC5 was highly expressed in tumor tissues compared to adjacent normal tissues (Fig. 2F). To determine the role of the ISG15-conjugating protein HERC5 in OSCC progression, we further examined protein expression for HERC5 in tumor and adjacent normal tissues from our hospital cohort of 8 patients. HERC5 protein expression was higher in OSCC tissues at baseline (Fig. 2G). Immunohistochemical results revealed that the positive expression site of HERC5 was mainly localized in the cytoplasm of tumor cells, and HERC5 expression was positively correlated with TNM-T stage (Fig. 2H).

Anti-metastatic role of HERC5 silencing in OSCC cells in vitro and in vivo

The basal expression levels of HERC5 in five OSCC cell lines were determined by the CCLE analysis. CAL27 cell lines exhibited the highest expression of HERC5, while SCC9 cells had the lowest expression (Fig. 1A). Stable overexpression of HERC5 was conducted in SCC9 cell strains by transfection of HERC5 expression plasmids (Fig. 1B and Supplementary Fig. 1A), while stable knockdown of HERC5 was carried out in CAL27 cell strains by the RNA interference system (Fig. 1C and supplementary Fig. 1B). Gain-of-function and loss-of-function experiments were then performed in SCC9 and CAL27 cells stably expressed HERC5. HERC5 overexpression facilitated the migratory ability and increased the number of cells invading through the matrigel-coated porous membrane in SCC9 cells (Fig. 1D). Highly expressed HERC5 also resulted in the loss of cell junctions mediated by the downregulation of E-cadherin and the upregulation of Vimentin (Fig. 1E), which allowed the cancer cells to freely migrate [20]. Silencing of HERC5 resulted in opposite alterations in CAL27 cells (Fig. 1D and E).

Next, stably transfected SCC9 and CAL27 cells marked with GFP were injected into nude mice by tail vein (Fig. 1F). After 8 weeks, metastasis of tumor in lung was viewed with whole-body fluorescent imaging system. The results showed that pulmonary metastasis was facilitated after overexpression of HERC5, yet inhibited after knockdown of HERC5 (Fig. 1G). Overexpression of HERC5 also increased metastatic nodules in the lung (Fig. 1H, arrows). Representative H&E images of SCC9 lung sections exhibited aggravated metastatic lung tumor burden following overexpression of HERC5 (Fig. 1I, arrowheads). Silencing of HERC5 resulted in the opposite results (Fig. 1G and I).

HERC5 depletion restores the cisplatin sensitivity and delays tumor growth

To investigate the effect of HERC5 on cisplatin-based chemosensitivity, stably transfected SCC9 and CAL27 cells were treated with dose-gradient cisplatin. MTT assay showed that overexpression of HERC5

weakened sensitivity of SCC9 cells to cisplatin, exhibited by increased cell viability (Fig. 3A). In line with this, knockdown of HERC5 enhanced cisplatin-based chemosensitivity in CAL27 cells (Fig. 3A). Next, cisplatin-induced cytotoxicity in OSCC cells (SCC9 and CAL27) was assessed based on release of LDH (Fig. 3B). Data showed that high expression of HERC5 attenuated the LDH release in SCC9 cells upon 6 μM

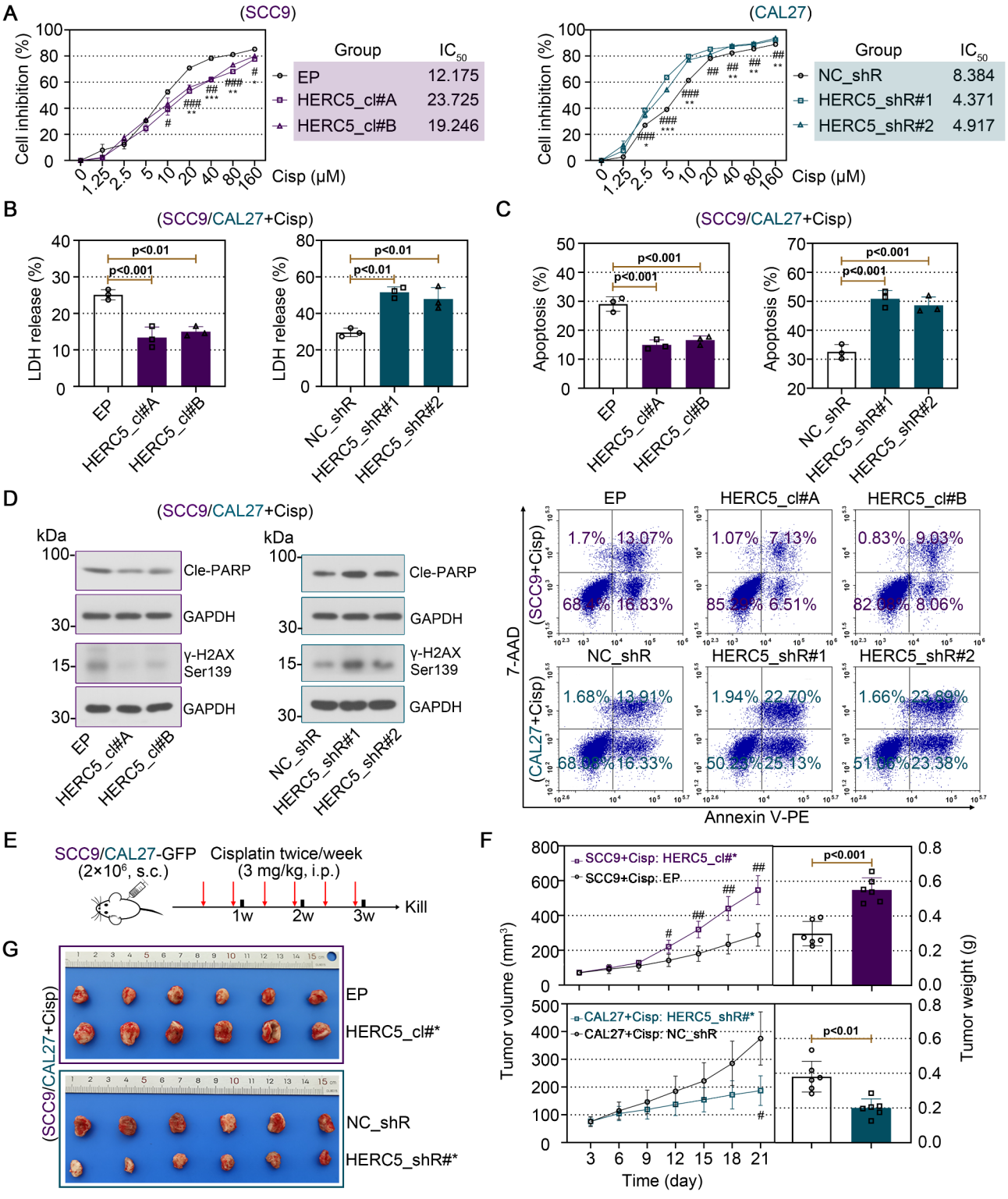

Fig. 3 (See legend on next page.)

(See figure on previous page.)

Fig. 3 HERC5 depletion restores the cisplatin sensitivity and delays tumor growth. (**A**). SCC9 (left) or CAL27 (right) cells cell stably expressing HERC5_cl/EP or HERC5_shR/NC_shR were treated with a gradient concentration of cisplatin for 48 h, after which cell growth inhibition was assessed by MTT assay. Treatment of SCC9 cells with 12 μM concentration of cisplatin showed 50% cell death. IC_{50} of cisplatin on CAL27 cells at this time was calculated to be 8 μM. (**B**). LDH release assays were performed to determine the ratio of LDH to total LDH in cell supernatants after 48 h of cisplatin treatment. 6 μM cisplatin for SCC. 4 μM cisplatin for CAL27. (**C**). Apoptosis of OSCC cells after 48 h of cisplatin treatment was determined by flow cytometer using Annexin V-PE/7-AAD assay. (**D**). Representative results of western blot analyses for γ-H2AX Ser139 and cleaved-PARP in SCC9 (left) or CAL27 (right) cells. (**E**). Schematic diagram of the experimental design. A total of 2×10^6 SCC9 or CAL27 cells stably expressing HERC5_cl/EP or HERC5_shR/NC_shR were injected subcutaneously (s.c.) into Balb/C nude mice. When tumors reached a volume of 50 mm^3, mice were injected intraperitoneally (i.p.) 3 mg/kg of cisplatin twice per week. Tumor volumes were recorded every three days. After 21 days, mice were killed and tumors were excised, and weighed. (**F**). Growth curve and weight of subcutaneous tumors. (**G**). Representative SCC9 (up) or CAL27 (down) xenograft tumors were shown. Data in (A, B, C, G) were expressed as mean values ± SD. # $p<0.05$, ## $p<0.01$ and ### $p<0.001$ for comparisons between HERC5_cl#A/HERC5_cl#*/HERC5_shR#1/HERC5_shR#* and EP/NC_shR. * $p<0.05$, ** $p<0.01$ and *** $p<0.001$ for comparisons between HERC5_cl#B/HERC5_shR#2 and EP/NC_shR

of cisplatin treatment, while low expression of HERC5 enhanced in CAL27 cells with 4 μM cisplatin. DNA damage and subsequent induction of apoptosis were considered as the primary cytotoxic mechanism of cisplatin [21, 22]. Therefore, we sought to determine whether the inhibition of DNA damage and apoptosis was involved in cisplatin resistance caused by HERC5 in OSCC cells. Flow cytometry analysis using Annexin V-E/7-AAD staining showed the percentage of apoptotic cells treated with cisplatin was remarkably reduced in HERC5-overexpressing SCC9 cells, yet increased in HERC5-silencing CAL27 cells (Fig. 3C). Immunoblotting data exhibited that overexpression of HERC5 in SCC9 cells substantially decreased cisplatin-induced PARP and γ-H2AX expression (Fig. 3D). Knocking down HERC5 yielded the opposite effect on cisplatin-induced PARP and γ-H2AX expression (Fig. 3D).

To evaluate the in vivo efficacy of HERC5 in cisplatin-based chemosensitivity, we generated SCC9 or CAL27 cell-derived tumor xenograft. When the xenograft grew to ~50 mm^3, cisplatin was intraperitoneally injected twice weekly for three weeks (Fig. 3E). Tumor growth curves showed that the tumor derived from HERC5-overexpressing SCC9 cells grew faster upon cisplatin treatment (Fig. 3F). After three weeks, the weights and volumes of tumors formed by SCC9/HERC5-OE cells were significantly larger than those of tumors derived from vector-control cells (Fig. 3F and G). Consistently, knockdown of HERC5 in CAL27 cells significantly delayed tumor growth in terms of both tumor volume and weight (Fig. 3F and G).

HERC5 enhances the stability of SNAI1 mRNA by inducing UGDH phosphorylation

The BioGRID interaction database revealed that UGDH was an interacting protein of ISG15 and its conjugating protein HERC5. Phosphorylation of UGDH at tyrosine 473 (pUGDH(Y473)) has previously been found to enhance the mRNA stability of SNAI1 and accelerate lung cancer metastasis [18] (Fig. 4B). Therefore, we examined the pUGDH(Y473) level in head and neck cancer (HNC) by Cancer Proteogenomic Data Analysis Site (cProSite) database. We found that the pUGDH(Y473)/total UGDH ratio was increased in HNC tissues (Fig. 4C). We subsequently performed western blot detection for tyrosine phosphorylation level of UGDH protein in OSCC and para-OSCC tissues from our hospital cohort. Data revealed that tyrosine phosphorylation level of UGDH was highly expressed in OSCC tissues (Fig. 4D). Furthermore, the expression of SNAI1, the downstream target of pUGDH(Y473), was also upregulated in OSCC tissues from our validation cohort (Fig. 4E and F).

Next, we sought to understand whether HERC5 affected SNAI1 expression via phosphorylating UGDH in OSCC cells. Overexpression of HERC5 enhanced stability and expression of SNAI1 mRNA in SCC9 cells (Fig. 4G and H). Highly expressed HERC5 also increased the tyrosine phosphorylation level of UGDH in SCC9 cells (Fig. 4I). Knockdown of HERC5 led to the opposite alteration (Fig. 4G-I). Moreover, silencing of UGDH reduced SNAI1 mRNA stability in HERC5-overexpressing SCC9 cells (Fig. 4J). UGDH (Y473F) mutation abrogated HERC5 OE-increased SNAI1 mRNA stability in SCC9 cells (Fig. 4K). Collectively, these data indicated that HERC5 enhanced the stability of SNAI1 mRNA by upregulating pUGDH(Y473) in OSCC cells.

HERC5 increases phosphorylation level of UGDH by ISGylation

Based on the above results, we supposed that HERC5-mediated UGDH phosphorylation might be associated with posttranslational ISGylation (Fig. 5A). The interaction between HERC5 and UGDH was observed in SCC9 and CAL27 cells via the Co-IP assay (Fig. 5B). The ISGylation cascade system was confirmed to exist in SCC9 and CAL27 cells by examining the expression levels of ISG15, E1 enzyme UBE1L, E2 enzyme UBCH8, and E3 ligase HERC5 via the CCLE analysis (Figs. 1A and 5C). UGDH ISGylation was enhanced after HERC5 overexpression, yet reduced after HERC5 silencing (Fig. 5D). HERC5 point mutant (C994A),

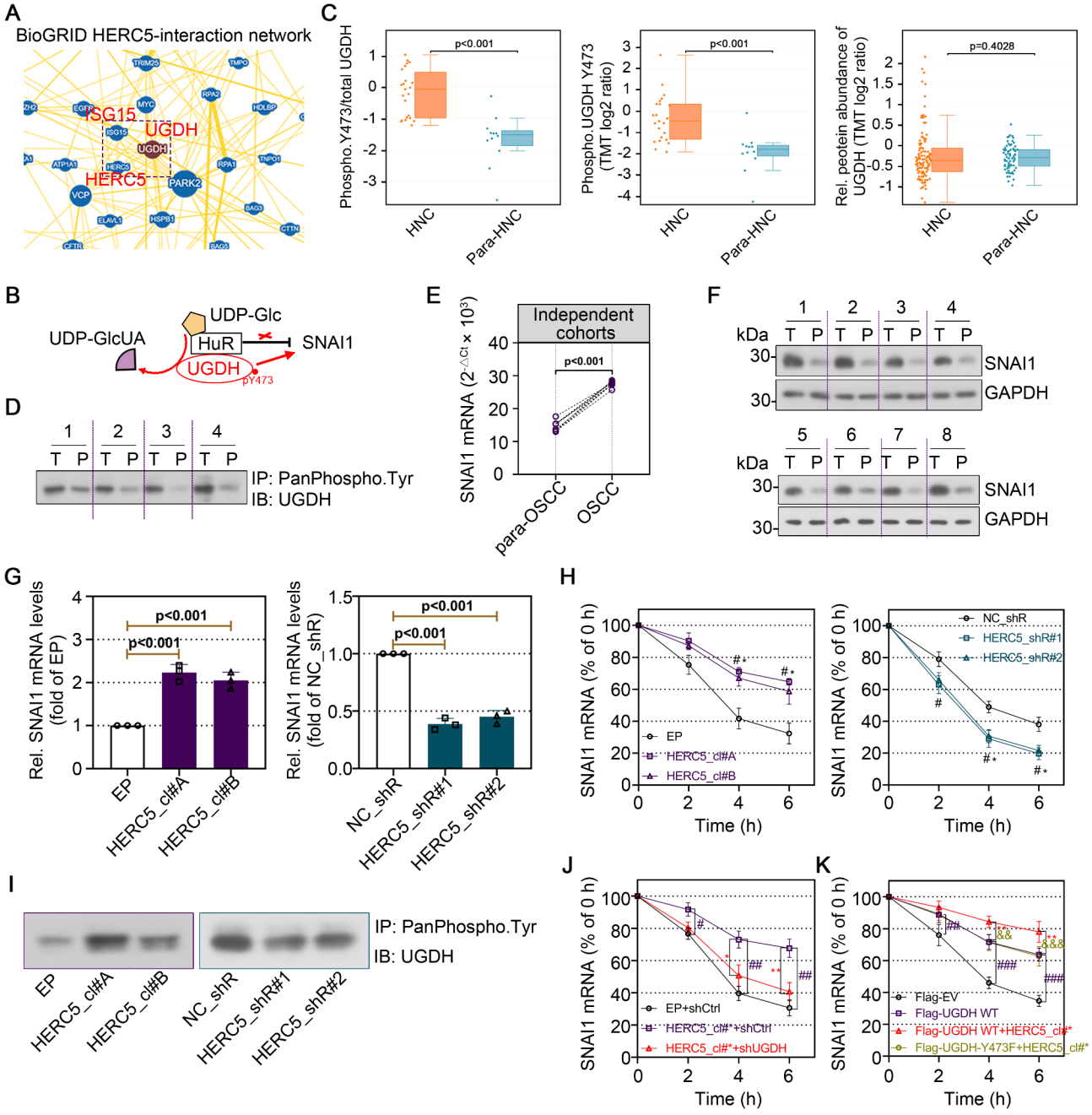

Fig. 4 HERC5 enhances the stability of SNAI1 mRNA by inducing UGDH phosphorylation. (**A**). Protein interaction network of human HERC5, as determined by BioGRID. Many HERC5-interacting proteins, including ISG15 and UGDH, were identified. (**B**). Schematic illustration of UGDH to promote EMT by increasing the stability of SNAI1 mRNA, as reported by Nature. 2019;571:127–131 [18]. UGDH, UDP-glucose 6-dehydrogenase. HuR, Hu antigen R. UDP-Glc, uridine diphosphate-glucose. UDP-GlcUA, UDP-glucuronic acid. (**C**). UGDH protein abundance, phosphorylation level at tyrosine 473, and ratio of Phospho.Y473/Total UGDH in head and neck cancer (HNC) and normal paracancerous tissues by Cancer Proteogenomic Data Analysis Site (cProSite). (**D**). Immunoprecipitation of tyrosine-phosphorylated proteins in lysates from OSCC and para-OSCC tissues, using a pan-phospho-Tyrosine antibody. Western blot analysis was performed using an anti-UGDH antibody to assess tyrosine phosphorylation levels of UGDH in OSCC vs. para-OSCC tissues. (**E**). SNAI1 mRNA expression levels in 8 paired OSCC and para-OSCC tissues of our independent hospital cohorts. (**F**). SNAI1 protein expression levels in 8 paired OSCC and para-OSCC tissues from our independent hospital cohorts. P, para-OSCC tissues. T, OSCC tissues. (**G**) Relative mRNA levels of SNAI1 in SCC9 (left) or CAL27 (right) cells. (**H**) SCC9 (left) or CAL27 (right) cells were treated with actinomycin D (1 μg/ml). Remained SNAI1 mRNA levels after treatment were examined at the indicated time points. (**I**). Immunoprecipitation of tyrosine-phosphorylated proteins in lysates from SCC9 (left) or CAL27 (right) cells, using an anti-pan-phospho-Tyrosine antibody. Western blot analysis was performed using an anti-UGDH antibody to assess tyrosine phosphorylation levels of UGDH. (**J**) Remained SNAI1 mRNA levels in SCC9 cells after treatment were examined at the indicated time points. (**K**). SCC9 cells stably overexpressing HERC5 were transiently transfected with pcDNA 3.1 (+) plasmids of a C-terminally Flag-tagged UGDH (wild type or Tyr473Phe (Y473F) mutant type). After 48 h, the remaining SNAI1 mRNA levels were examined at the indicated time points. Data in (G, H, J, K) were expressed as mean values ± SD. #/*/& $p < 0.05$, ##/**/&& $p < 0.01$ and ###/***/&&& $p < 0.001$

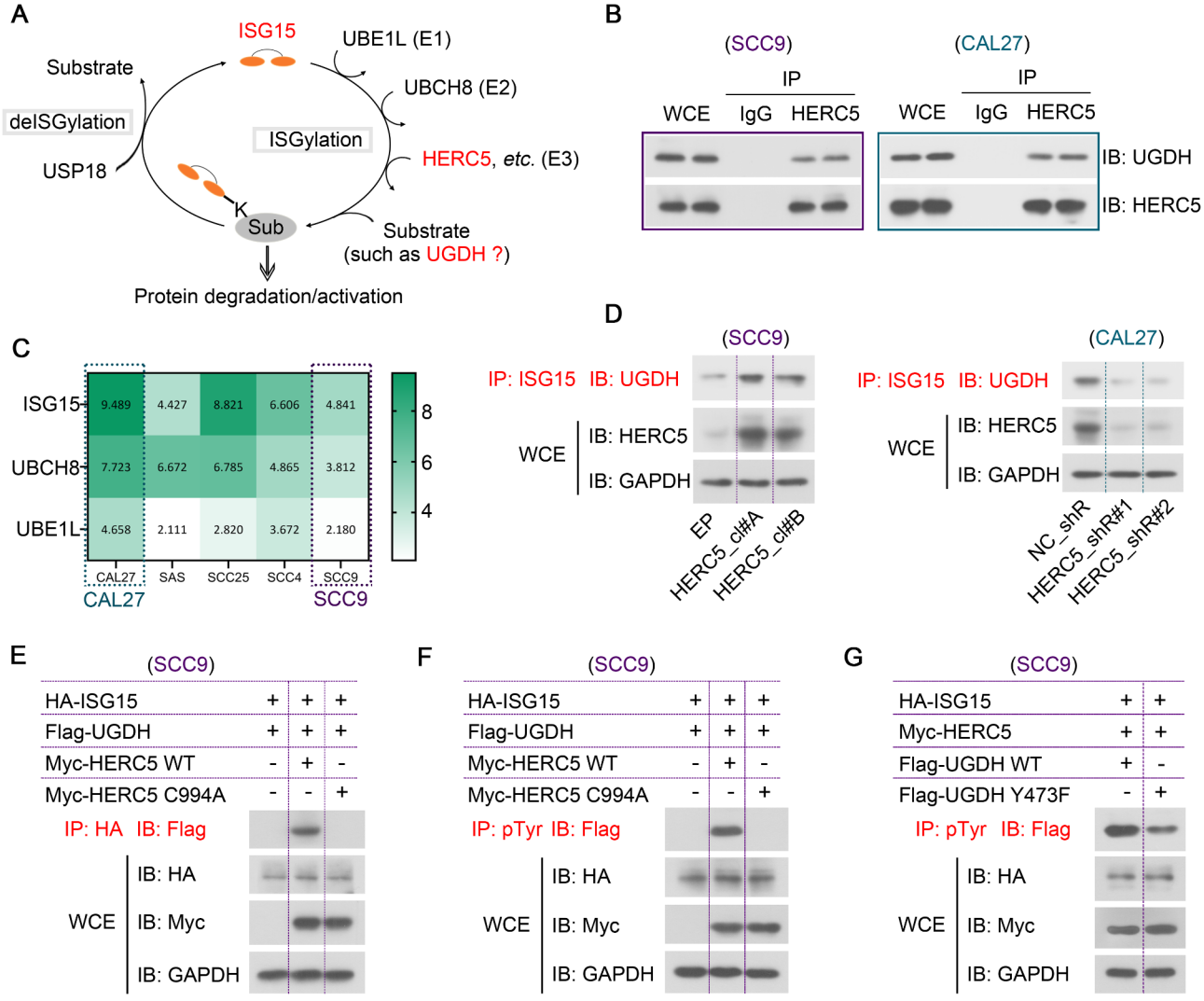

Fig. 5 HERC5 increases phosphorylation level of UGDH by ISGylation. (**A**). The cascade reactions of ISGylation. The covalent modification of ISG15 requires an E1 activating enzyme (UBE1L), an E2 conjugating enzyme (UBCH8) and one of three E3 ligases (such as HERC5). Finally, ISG15 links to the Lys (K) residue of the target protein and mediates a ubiquitin-like modification. (**B**). Co-IP results. Whole-cell extracts (WCE) from SCC9 (up) or CAL27 (down) cells were subjected to immunoprecipitation with an antibody against HERC5 or a control IgG. Bound proteins were detected by western blot analysis. (**C**). Heatmap using the CCLE dataset for mRNA expression of ISG15 and its conjugation enzymes, including E1 enzyme UBE1L and E2 enzyme UBCH8, in five OSCC cells (CAL27, SAS, SCC25, SCC4, and SCC9). (**D**). Immunoprecipitation of tyrosine-phosphorylated proteins in lysates from SCC9 (left) or CAL27 (right) cells, using an anti-ISG15 antibody. Western blot analysis was performed using an anti-UGDH antibody to assess ISGylation of UGDH. **(E&F)**. SCC9 cells were transiently transfected with pcDNA3.1-HA-ISG15, pcDNA3.1-Flag-UGDH and pcDNA3.1-Myc-HERC5 (wild type or Cys994Ala mutant type) plasmids. After 48 h, WCE were subjected to immunoprecipitation with an antibody against HA (E) and pan-phospho-Tyrosine (F). Bound proteins were detected by western blot analysis. (**G**). SCC9 cells were transiently transfected with pcDNA3.1-HA-ISG15, pcDNA3.1-Myc-HERC5 and pcDNA3.1-Flag-UGDH (wild type or Tyr473Phe mutant type) plasmids. After 48 h, WCE were subjected to immunoprecipitation with an anti-pan-phospho-Tyrosine antibody. Bound proteins were detected by western blot analysis

which lost its E3 ISGylation ligase activity, did not induce the UGDH ISGylation (Fig. 5E), indicating that HERC5 promoted ISGylation of UGDH via its E3 ligase activity. We also analyzed the effect of HERC5 E3 ISGylation ligase activity on UGDH tyrosine phosphorylation. It has been known that substitution of Cys-994 to Ala (C994A) in the HECT domain of HERC5 completely abrogates its E3 ligase activity [23]. Here, we observed that HERC5 (C994A) mutation inhibited the tyrosine phosphorylation of UGDH (Fig. 5F), indicating the critical C994 in the HECT domain of HERC5 was indispensable for potentiating UGDH activity. After UDGH (Y473F) mutation, the tyrosine phosphorylation of UDGH promoted by ISGylation was impaired (Fig. 5G).

SNAI1 depletion inhibits HERC5 OE-induced cell invasion and cisplatin resistance

We construct SNAI1 shRNA to transfect SCC9 cells stably expressing HERC5. Real-time PCR and western blot results revealed that knockdown of SNAI1 effectively downregulated HERC5 OE-increased SNAI1 expression (Fig. 6A and B). HERC5 overexpression-induced cell invasion was inhibited after silencing of SNAI1 (Fig. 6C and D). In addition, SNAI1 depletion abrogated HERC5 overexpression-mediated suppression of cell apoptosis upon cisplatin treatment (Fig. 6E), indicating that SNAI1 was required for HERC5 OE-caused cisplatin resistance.

Discussion

The high mortality rate of OSCC, as its aggressive and recurrent potential, remains a challenge in clinical practice. Comprehensive elucidation of the possible molecular mechanisms regarding the malignant progression and chemoresistance of OSCC is a cornerstone of developing effective therapeutic strategies. In this study, we identify that HERC5 acts as an ISGylation E3 ligase for UGDH and induces its phosphorylation, resulting in UGDH activation. Knockdown of HERC5 reduces UGDH activity and therefore inhibits SNAI1-caused tumor metastasis and cisplatin resistance in OSCC. This study highlights the important function of human HERC family, such as HERC5, in OSCC development.

The human HERC family contains six members who are categorized into two subfamilies: (1) large HERCs (HERC1-2) with one HECT domain and multiple RCC1-like domain (RLD), and (2) small HERCs (HERC3-6) with single HECT and RLD domains. The HECT domain can act as ubiquitin/ubiquitin-like protein ligase, while the RLD domain is involved in cell

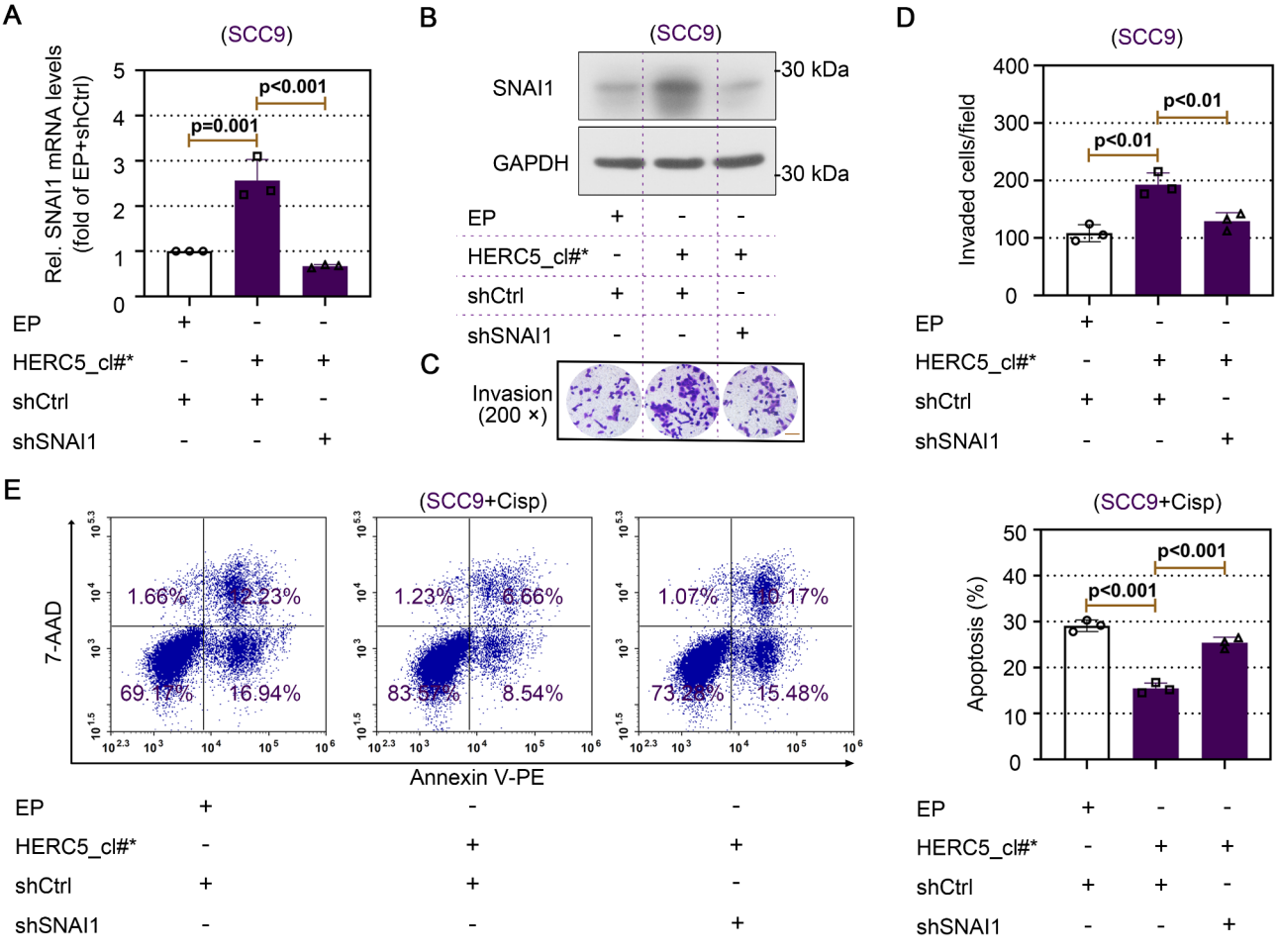

Fig. 6 SNAI1 depletion inhibits HERC5 OE-induced cell invasion and cisplatin resistance. (**A&B**). A shRNA targeting HERC5 mRNA (shSNAI1) and non-targeting control shRNA (shCtrl) was inserted in pRNA-H1.1/Neo plasmid. The plasmids were transfected into SCC9 cells. After 48 h, expression of SNAI1 mRNA (A) and protein (B) were detected by real-time PCR and western blot analyses. (**C&D**). Transwell matrigel invasion assays in SCC9 cells. Representative photomicrographs (C, Scale bars: 100 μm) and quantification (D) of the invasive cells (stained with crystal violet) at 24 h in lower surface of Transwell chamber. (**E**). 48 h after transfection, SCC9 cells were treated with 6 μM of cisplatin. Apoptosis of SCC9 cells after 48 h of cisplatin treatment was determined by flow cytometer using Annexin V-PE/7-AAD assay. Data in (A, D, E) were expressed as mean values ± SD

cycle regulation [24]. Growing body of evidence has demonstrated that the HERC proteins are engaged in tumorigenesis, excluding OSCC [25]. Data available from the GEO online public database showed that only HERC5 was differentially expressed in OSCC tissues and cell lines (Fig. 2A). HERC5 was early described as a functionally active HECT ubiquitin ligase, and required the E2 ubiquitin-conjugating enzyme UbcH5a for its activity [26]. In addition to transferring ubiquitin, HERC5 was later identified as the E3 ligase for conjugation of ISG15 (ISGylation) [27]. HERC5 plays a vital role in cancer development and progression by regulating a lot of proteins implicated in pathophysiological processes via posttranslational modification. HERC5-mediated ISGylation of Carboxy Terminus Of Hsp70-Interacting Protein (CHIP; also STUB1) promoted its activity and therefore inhibited non-small cell lung cancer (NSCLC) cell growth [28]. Apart from that, it was recently reported to act as a metastasis suppressor gene in NSCLC through altering the metabolic state of cells, which was independent of its ISGylation function [29]. In breast cancer, HERC5 accelerated cell proliferation and migration through facilitating ISGylation-dependent Interferon Gamma Inducible Protein 16 (IFI16) degradation [11]. Silencing of HERC5 inhibited breast cancer cell proliferation [30]. In contradiction to the above research on breast cancer, a new study published by Tian et al. showed that HERC5 led to ubiquitinated degradation of Y-Box Binding Protein 1 (YBX1) oncoprotein in breast cancer cells [31]. HERC5 was also essential for ISG15-induced degradation of p53 tumor suppressor [12, 32]. Lund et al. revealed that HERC5 was a potential key driver of cisplatin resistance in ovarian cancer, indicating its importance in malignant transformation of ovarian cancer [13]. HERC5 can exert either a tumor-promoting or tumor-inhibitory role, depending on cancer types and interacting proteins. We here note that UbcH5a expression in OSCC tissues was not significantly changed compared with the control group, by retrieving the data from the GEO public database. Therefore, HERC5 overexpression facilitated metastasis and cisplatin resistance of OSCC, which may be at least partly due to its ISGylation function, not its ubiquitylation. It was documented that HERC5 and ISG15 expression were upregulated by glycoprotein 90 K (also LGALS3BP, MAC-2-BP) in HeLa cervical cancer cells and CSC221 colorectal adenocarcinoma-enriched cancer stem cells [33]. LGALS3BP was higher in primary OSCC tumor tissues than in paired normal oral mucosae, and LGALS3BP depletion induced growth inhibition and apoptosis [34]. We believe that HERC5-mediated ISGylation in OSCC may be affected by LGALS3BP.

Activation of EGFR led to excess accumulation of toxic UDP-GlcUA, which was produced by UGDH phosphorylation [16]. A study has reported that the expression rate of EGFR in OSCC is up to 73% [35]. This may be responsible for high phosphorylation levels of UGDH in OSCC, even if overall levels were not changed. In addition, chemoresistant subpopulations of lung cancer and triple-negative breast cancer cells through cisplatin exposure displayed robust induction of UGDH [36]. We propose that activation of UGDH in OSCC may be correlated with increased resistance to drugs. As a key rate-limiting enzyme in the glucuronate pathway, UGDH was also correlated with increased metastatic potential in cancers [18, 37]. A previous study demonstrated that Krüppel-Like Factor 4 (KLF4) activated UGDH transcription in a mCpG-dependent manner, and knockdown of UGDH inhibited KLF4 overexpression-caused tumor growth and migration [17]. Pharmacological inhibition of UGDH activity delayed prostate and thyroid cancer cell proliferation [38]. In the present study, we identified a novel way in which HERC5-catalyzed ISGylation reduces UGDH activity. UGDH is known to enhance the binding of HuR to SNAI1 mRNA by converting UDP-Glc to UDP-GlcUA (Fig. 4B) [18]. HuR is a ubiquitously expressed RNA-binding protein that binds to the 3'-untranslated region (UTR) within mRNAs and increases their stability [39]. In OSCC, motile and invasive capabilities of tumor cells were reduced upon HuR depletion [40]. Therefore, it is reasonable that the oncogenicity is diminished in HERC5-overexpressing OSCC cells after silencing of SNAI1.

Similar to ubiquitination, ISGylation is an enzymatic cascade reaction requiring the E1 activating enzyme UBE1L, the E2 binding enzyme UBCH8, and the E3 ligases HERC5, ARIH1, and TRIM25 [3]. This process is reversible and counteracted by deISGylating enzyme Ubiquitin-Specific Peptidase 18 (USP18) (Fig. 5A) [6]. We have confirmed that E3 HERC5 induces UGDH phosphorylation in the presence of the complete ISG15 conjugation system (with ISG15, E1 UBE1L, and E2 UBCH8). It arouses our attention whether UGDH activity is affected by other E3 ISGylation ligases. Apart from the HERC5, we see an interaction between UGDH and another E3 ligase TRIM25 in the BioGRID interaction database. Unfortunately, no significant change in TRIM25 expression was observed in numerous microarray data of OSCC tissues/cells and normal tissues/cells (Fig. 2A). In addition, despite the presence of endogenous USP18 in OSCC cells [41], debinding role of USP18 does not interfere with HERC5 OE-mediated UGDH ISGylation. Taken together, our results demonstrate that HERC5 functions as the only E3 ligase for UGDH ISGylation and positively

regulates metastasis and cisplatin resistance in OSCC cells.

High-risk human HPV infection is one of the leading causes of OSCC [42]. HPV infection helps the body evade interferon-mediated immune responses [43]. In addition, the immune- and interferon-response involved in these neoplasms differs based on "hotness" of the tumors. "Hot" tumors are characterized by significant high infiltration of T cells that may predispose to activate the interferon signaling pathway, thus promoting the generation of more interferon-stimulated genes [44]. Basal levels of ISG15 are weakly in six HPV-negative OSCC cells (OECM1, CGHNC9, TW2.6, HSC3, SAS and OC3) from previous research [9], and are not detected in two HPV-negative OSCC cells (SCC-9 and CAL-27) from this study (Supplementary Fig. 2A). Expression of ISG15 as a conjugated or free protein can be substantially increased under stimulation with interferon [4]. Whether HPV infection and/or effector T cell infiltration affects availabilities of ISG15 as substrate for the ISGylation and subsequent cancer progression remain unknown. Further studies are warranted for assessment of the impact of HPV status and tumor immune microenvironment on ISGylation.

Conclusions

In summary, we uncover a previously unrecognized mechanism by which HERC5-mediated ISGylation induces UGDH activation and therefore promotes OSCC metastasis and cisplatin resistance by enhancing the stability of SNAI1 mRNA. Although further evaluation in future studies is needed, our study indicates that targeting HERC5 may be a promising strategy for OSCC therapy.

Supplementary Information

The online version contains supplementary material available at https://doi.org/10.1186/s13062-025-00622-1.

Supplementary Material 1

Acknowledgements
Not applicable.

Author contributions
XZ: Conceptualization, Methodology, Formal analysis, Investigation, Funding acquisition, Writing-Original draft. FL, QF and CS: Formal analysis, Investigation. JF: Writing-reviewing & editing.

Funding
This research was funded by the Medical Science and Technology Research Plan (Joint Construction) of Health Commission of Henan Province (LHGJ20230083) and Project of Science and Technology Research of Science and Technology Department of Henan Province (222102310364).

Data availability
No datasets were generated or analysed during the current study.

Declarations

Ethics approval and consent to participate
Human tissue samples were processed following standard operating procedures with the approval by the Ethical and Scientific Committees of Henan Cancer Hospital (Approval No. 2022-07-01), and obtained informed consent.

Consent for publication
Not applicable.

Competing interests
The authors declare no competing interests.

Received: 13 November 2024 / Accepted: 22 February 2025
Published online: 05 March 2025

References

1. Bray F, Ferlay J, Soerjomataram I, Siegel RL, Torre LA, Jemal A. Global cancer statistics 2018: GLOBOCAN estimates of incidence and mortality worldwide for 36 cancers in 185 countries. CA Cancer J Clin. 2018;68(6):394–424.
2. Sasahira T, Kirita T. Hallmarks of cancer-related newly prognostic factors of oral squamous cell carcinoma. Int J Mol Sci. 2018;19(8).
3. Yuan Y, Qin H, Li H, Shi W, Bao L, Xu S, et al. The functional roles of ISG15/ISGylation in cancer. Molecules. 2023;28(3):1337.
4. Bolado-Carrancio A, Lee M, Ewing A, Muir M, Macleod KG, Gallagher WM, et al. ISGylation drives basal breast tumour progression by promoting EGFR recycling and Akt signalling. Oncogene. 2021;40(44):6235–47.
5. Xue X, Tian X, Zhang C, Miao Y, Wang Y, Peng Y, et al. YAP isgylation increases its stability and promotes its positive regulation on PPP by stimulating 6PGL transcription. Cell Death Discov. 2022;8(1):59.
6. Mustachio LM, Kawakami M, Lu Y, Rodriguez-Canales J, Mino B, Behrens C, et al. The ISG15-specific protease USP18 regulates stability of PTEN. Oncotarget. 2017;8(1):3–14.
7. Alcala S, Sancho P, Martinelli P, Navarro D, Pedrero C, Martin-Hijano L, et al. ISG15 and isgylation is required for pancreatic cancer stem cell mitophagy and metabolic plasticity. Nat Commun. 2020;11(1):2682.
8. Zhou MJ, Chen FZ, Chen HC, Wan XX, Zhou X, Fang Q, et al. ISG15 inhibits cancer cell growth and promotes apoptosis. Int J Mol Med. 2017;39(2):446–52.
9. Chen YL, Wu WL, Jang CW, Yen YC, Wang SH, Tsai FY, et al. Interferon-stimulated gene 15 modulates cell migration by interacting with Rac1 and contributes to lymph node metastasis of oral squamous cell carcinoma cells. Oncogene. 2019;38(23):4480–95.
10. Chu L, Qian L, Chen Y, Duan S, Ding M, Sun W, et al. HERC5-catalyzed isgylation potentiates cGAS-mediated innate immunity. Cell Rep. 2024;43(3):113870.
11. Liu C, Li L, Hou G, Lu Y, Gao M, Zhang L. HERC5/IFI16/p53 signaling mediates breast cancer cell proliferation and migration. Life Sci. 2022;303:120692.
12. Wang Y, Ding Q, Xu T, Li CY, Zhou DD, Zhang L. HZ-6d targeted HERC5 to regulate p53 isgylation in human hepatocellular carcinoma. Toxicol Appl Pharmacol. 2017;334:180–91.
13. Lund RJ, Huhtinen K, Salmi J, Rantala J, Nguyen EV, Moulder R, et al. DNA methylation and transcriptome changes associated with cisplatin resistance in ovarian cancer. Sci Rep. 2017;7(1):1469.
14. Reddy RB, Khora SS, Suresh A. Molecular prognosticators in clinically and pathologically distinct cohorts of head and neck squamous cell carcinoma-a meta-analysis approach. PLoS ONE. 2019;14(7):e0218989.
15. Egger S, Chaikuad A, Kavanagh KL, Oppermann U, Nidetzky B. UDP-glucose dehydrogenase: structure and function of a potential drug target. Biochem Soc Trans. 2010;38(5):1378–85.
16. Teoh ST, Ogrodzinski MP, Lunt SY. UDP-glucose 6-dehydrogenase knockout impairs migration and decreases in vivo metastatic ability of breast cancer cells. Cancer Lett. 2020;492:21–30.
17. Oyinlade O, Wei S, Lal B, Laterra J, Zhu H, Goodwin CR, et al. Targeting UDP-alpha-D-glucose 6-dehydrogenase inhibits glioblastoma growth and migration. Oncogene. 2018;37(20):2615–29.
18. Wang X, Liu R, Zhu W, Chu H, Yu H, Wei P, et al. UDP-glucose accelerates SNAI1 mRNA decay and impairs lung cancer metastasis. Nature. 2019;571(7763):127–31.

19. Hsu DS, Lan HY, Huang CH, Tai SK, Chang SY, Tsai TL, et al. Regulation of excision repair cross-complementation group 1 by snail contributes to cisplatin resistance in head and neck cancer. Clin Cancer Res. 2010;16(18):4561–71.
20. Chaw SY, Abdul Majeed A, Dalley AJ, Chan A, Stein S, Farah CS. Epithelial to mesenchymal transition (EMT) biomarkers–E-cadherin, beta-catenin, APC and Vimentin–in oral squamous cell carcinogenesis and transformation. Oral Oncol. 2012;48(10):997–1006.
21. Chou AJ, Gorlick R. Chemotherapy resistance in osteosarcoma: current challenges and future directions. Expert Rev Anticancer Ther. 2006;6(7):1075–85.
22. Zajaczkowska R, Kocot-Kepska M, Leppert W, Wrzosek A, Mika J, Wordliczek J. Mechanisms of chemotherapy-induced peripheral neuropathy. Int J Mol Sci. 2019;20(6).
23. Wong JJ, Pung YF, Sze NS, Chin KC. HERC5 is an IFN-induced HECT-type E3 protein ligase that mediates type I IFN-induced isgylation of protein targets. Proc Natl Acad Sci U S A. 2006;103(28):10735–40.
24. Sanchez-Tena S, Cubillos-Rojas M, Schneider T, Rosa JL. Functional and pathological relevance of HERC family proteins: a decade later. Cell Mol Life Sci. 2016;73(10):1955–68.
25. Mao X, Sethi G, Zhang Z, Wang Q. The emerging roles of the HERC ubiquitin ligases in cancer. Curr Pharm Des. 2018;24(15):1676–81.
26. Kroismayr R, Baranyi U, Stehlik C, Dorfleutner A, Binder BR, Lipp J. HERC5, a HECT E3 ubiquitin ligase tightly regulated in LPS activated endothelial cells. J Cell Sci. 2004;117(Pt 20):4749–56.
27. Dastur A, Beaudenon S, Kelley M, Krug RM, Huibregtse JM. Herc5, an interferon-induced HECT E3 enzyme, is required for conjugation of ISG15 in human cells. J Biol Chem. 2006;281(7):4334–8.
28. Yoo L, Yoon AR, Yun CO, Chung KC. Covalent ISG15 conjugation to CHIP promotes its ubiquitin E3 ligase activity and inhibits lung cancer cell growth in response to type I interferon. Cell Death Dis. 2018;9(2):97.
29. Schneegans S, Loptien J, Mojzisch A, Loreth D, Kretz O, Raschdorf C, et al. HERC5 downregulation in non-small cell lung cancer is associated with altered energy metabolism and metastasis. J Exp Clin Cancer Res. 2024;43(1):110.
30. Tang J, Yang Q, Cui Q, Zhang D, Kong D, Liao X, et al. Weighted gene correlation network analysis identifies RSAD2, HERC5, and CCL8 as prognostic candidates for breast cancer. J Cell Physiol. 2020;235(1):394–407.
31. Tian W, Zhu L, Luo Y, Tang Y, Tan Q, Zou Y et al. Autophagy deficiency induced by SAT1 potentiates tumor progression in triple-negative breast cancer. Adv Sci (Weinh). 2024;11(36):e2309903.
32. Huang YF, Bulavin DV. Oncogene-mediated regulation of p53 isgylation and functions. Oncotarget. 2014;5(14):5808–18.
33. Park SY, Yoon S, Kim H, Kim KK. 90K glycoprotein promotes degradation of mutant beta-catenin lacking the isgylation or phosphorylation sites in the N-terminus. Neoplasia. 2016;18(10):618–25.
34. Endo H, Muramatsu T, Furuta M, Uzawa N, Pimkhaokham A, Amagasa T, et al. Potential of tumor-suppressive miR-596 targeting LGALS3BP as a therapeutic agent in oral cancer. Carcinogenesis. 2013;34(3):560–9.
35. Laimer K, Spizzo G, Gastl G, Obrist P, Brunhuber T, Fong D, et al. High EGFR expression predicts poor prognosis in patients with squamous cell carcinoma of the oral cavity and oropharynx: a TMA-based immunohistochemical analysis. Oral Oncol. 2007;43(2):193–8.
36. Doshi MB, Lee N, Tseyang T, Ponomarova O, Goel HL, Spears M, et al. Disruption of sugar nucleotide clearance is a therapeutic vulnerability of cancer cells. Nature. 2023;623(7987):625–32.
37. Gao Q, Cheng B, Chen C, Lei C, Lin X, Nie D, et al. Dysregulated glucuronic acid metabolism exacerbates hepatocellular carcinoma progression and metastasis through the TGFbeta signalling pathway. Clin Transl Med. 2022;12(8):e995.
38. Scoglio S, Lo Curcio V, Catalani S, Palma F, Battistelli S, Benedetti S. Inhibitory effects of aphanizomenon flos-aquae constituents on human UDP-glucose dehydrogenase activity. J Enzyme Inhib Med Chem. 2016;31(6):1492–7.
39. Weisse J, Rosemann J, Krauspe V, Kappler M, Eckert AW, Haemmerle M, et al. RNA-binding proteins as regulators of migration, invasion and metastasis in oral squamous cell carcinoma. Int J Mol Sci. 2020;21:18.
40. Kakuguchi W, Kitamura T, Kuroshima T, Ishikawa M, Kitagawa Y, Totsuka Y, et al. HuR knockdown changes the oncogenic potential of oral cancer cells. Mol Cancer Res. 2010;8(4):520–8.
41. AbdulMajeed AA, Dalley AJ, Farah CS. Loss of ELF3 immunoexpression is useful for detecting oral squamous cell carcinoma but not for distinguishing between grades of epithelial dysplasia. Ann Diagn Pathol. 2013;17(4):331–40.
42. Ramqvist T, Dalianis T. An epidemic of oropharyngeal squamous cell carcinoma (OSCC) due to human papillomavirus (HPV) infection and aspects of treatment and prevention. Anticancer Res. 2011;31(5):1515–9.
43. Lei V, Petty AJ, Atwater AR, Wolfe SA, MacLeod AS. Skin viral infections: host antiviral innate immunity and viral immune evasion. Front Immunol. 2020;11:593901.
44. Wang L, Geng H, Liu Y, Liu L, Chen Y, Wu F et al. Hot and cold tumors: immunological features and the therapeutic strategies. MedComm (2020). 2023;4(5):e343.

Publisher's note